Published in final edited form as:
Mol Genet Metab. 2011 November ; 104(3): 346–355. doi:10.1016/j.ymgme.2011.04.019.

Alterations in Membrane Caveolae and BK_{Ca} Channel Activity in Skin Fibroblasts in Smith-Lemli-Opitz Syndrome

Gongyi Ren[1], **Robert F. Jacob**[2], **Yuri Kaulin**[3], **Paul DiMuzio**[2], **Yi Xie**[1], **R. Preston Mason**[2,4], **G. Stephen Tint**[5], **Robert D. Steiner**[6], **Jean-Baptiste Roulett**[6], **Louise Merkens**[6], **Diana Whitaker-Mendez**[7], **Phillipe G. Frank**[7], **Michael Lisanti**[7], **Robert H. Cox**[8], and **Thomas N. Tulenko**[1]

[1]Department of Surgery, Cooper University Hospital, Camden, NJ

[2]Elucida Research LLC, Beverly, MA, Department of Surgery, Thomas Jefferson University College of Medicine, Philadelphia, PA

[3]Department of Anatomy and Cell Biology, Thomas Jefferson University College of Medicine, Philadelphia, PA

[4]Brigham & Women's Hospital, Harvard Medical School, Boston, MA

[5]Research Service, Department of Veterans Affairs Medical Center, East Orange, NJ and Department of Medicine, UMDNJ-New Jersey Medical School, Newark, NJ

[6]Departments of Pediatrics and Molecular & Medical Genetics, Child Development and Rehabilitation Center, Doernbecher Children's Hospital, Oregon Health & Science University, Portland, OR

[7]Department of Stem Cell Biology & Regenerative Medicine, and Cancer Biology, Thomas Jefferson University College of Medicine, Philadelphia, PA

[8]Lankenau Institute for Medical Research, Wynnewood, PA

Abstract

The Smith-Lemli-Opitz syndrome (SLOS) is an inherited disorder of cholesterol synthesis caused by mutations in *DHCR7* which encodes the final enzyme in the cholesterol synthesis pathway. The immediate precursor to cholesterol synthesis, 7-dehydrocholesterol (7-DHC) accumulates in the plasma and cells of SLOS patients which has led to the idea that the accumulation of abnormal sterols and/or reduction in cholesterol underlies the phenotypic abnormalities of SLOS. We tested the hypothesis that 7-DHC accumulates in membrane caveolae where it disturbs caveolar bilayer structure-function. Membrane caveolae from skin fibroblasts obtained from SLOS patients were isolated and found to accumulate 7-DHC. In caveolar-like model membranes containing 7-DHC, subtle, but complex alterations in intermolecular packing, lipid order and membrane width were observed. In addition, the BK_{Ca} K^+ channel, which co-migrates with caveolin-1 in a membrane fraction enriched with cholesterol, was impaired in SLOS cells as reflected by reduced single channel conductance and a 50 mV rightward shift in the channel activation voltage. In addition, a

Address correspondence to: Thomas N. Tulenko, Ph.D., Department of Surgery, Cooper University Hospital, 3 Cooper Plaza, Suite 411, Camden, NJ 08103, 856-757-9646 (Phone), 856-757-9647 (FAX), tulenko-thomas@cooperhealth.edu.
Y.X. Current Address: Diabetes Section, Laboratory of Clinical Investigation, National Institute on Aging, NIH, Baltimore, MD.

marked decrease in BK_{Ca} protein but not mRNA expression levels were seen suggesting post-translational alterations. Accompanying these changes was a reduction in caveolin-1 protein and mRNA levels, but membrane caveolar structure was not altered. These results are consistent with the hypothesis that 7-DHC accumulation in the caveolar membrane results in defective caveolar signaling. However, additional cellular alterations beyond mere changes associated with abnormal sterols in the membrane likely contribute to the pathogenesis of SLOS.

Keywords

7-dehydrocholesterol; β-hydroxy-steroid-Δ^7-reductase (DHCR7); birth defects; caveolin-1; lipid rafts; membrane structure/function

Introduction

Smith-Lemli-Opitz syndrome (SLOS) is an autosomal recessive disorder of cholesterol biosynthesis caused by mutations in the gene that encodes 3β-hydroxysterol-Δ^7-reductase (DHCR7), the final enzyme in the cholesterol biosynthetic pathway. Affected individuals exhibit multiple anatomic malformations and mental retardation, though the phenotypic expression of this condition is extremely variable. The clinical features of SLOS are thought to be primarily related to cholesterol deficiency and/or accumulation of cholesterol precursors and their metabolites. The primary metabolite that accumulates in SLOS is the immediate precursor to cholesterol in the Kandutsch-Russell cholesterol synthesis pathway, 7-dehydrocholesterol (7-DHC) [1–2]. 7-DHC contains a double bond at carbon seven, which is reduced by DHCR7 to form unesterified (free) cholesterol (FC), but is otherwise structurally identical to FC (Figure 1). Tint *et al.* [2] first described the biochemical defect in SLOS patients by virtue of accumulation of 7-DHC in plasma of affected individuals. This finding has become diagnostic for SLOS and has led to the detailed description of a large variety of *DHCR7* mutations with over 130 reported to date and which may explain the large phenotypic variation observed for this disorder [3–4]. In contrast with the genetics of SLOS, relatively little work has been done to address the cell biology of this debilitating disease. The discovery that 7-DHC accumulation might participate in the pathogenesis of SLOS stems from the early work of Honda *et al.* [5] who first demonstrated that 7-DHC accumulates in skin fibroblasts cultured from patients with SLOS. This observation was confirmed by Wassif *et al.* [6], and extended by us in a study demonstrating that cell membranes from SLOS fibroblasts contain 7-DHC and are also dysfunctional [7].

Cell membranes are well known to be highly dependent on the presence of cholesterol for normal structure and function. Cholesterol contains a hydrophobic sterol ring with a saturated hydrocarbon side chain attached to carbon 17 which contributes to its profound lipophilicity. Hence, its preferred environment is in the fatty acyl chain region of cell membranes where it readily associates with sphingomyelin by virtue of hydrogen bonding to sphingomyelin's saturated fatty acyl chains. Together, cholesterol and sphingomyelin tend to coalesce by phase separation into liquid ordered domains within the plane of the membrane bilayer to form "cholesterol rafts" [8]. A subset of these lipid rafts incorporate caveolin, the signature protein of caveolae [9] which binds tightly to cholesterol and is thought to account for the formation of flask-shaped invaginations in the membrane [10]. Caveolin contains a single hairpin loop comprised of lipophilic amino acid residues which bind to cholesterol while the amino and carboxyl ends of caveolin orient to the cytosolic side of the membrane. Caveolin in turn binds a large number of proteins of considerable importance to cell function, including ion channels, ion transporters, G-protein coupled receptors, lipid (and cholesterol) transporters and signaling cascades, most of which appear to be regulated, at least in part, by caveolin [11]. Caveolin has thus come to be appreciated

as a scaffolding protein within the caveolar complex which functions as an important signaling module in the cell membrane mediating a host of signaling and transport activities essential to the health of a large variety of cells.

Since 7-DHC is present in the cell membranes of SLOS patients [7], it is plausible that its presence may disturb membrane function. Supporting a disrupting action of 7-DHC on membrane function are the recent observations by Singh, *et al.*, [12] that the incorporation of 7-DHC into membranes containing the serotonin$_{1A}$ receptor alters ligand binding. In addition, the potential for 7-DHC to insert into and disturb cell membranes and perhaps membrane caveolae has been suggested by various studies using model membranes [13–15] and cell cultures [16–17] in which exogenous cholesterol precursors are added directly to experimental preparations, or in rats treated with DHCR7 inhibitors [18]. While these studies show alterations consistent with membrane disturbances, their relevance to membrane function in humans harboring *DHCR7* mutations is not clear.

Considering the importance of caveolar function to normal cell biology, we sought to determine the degree to which 7-DHC might accumulate in the caveolar membrane and disturb caveolar function in SLOS patients. Herein we present results demonstrating that 7-DHC accumulates in the caveolar membrane which is accompanied by alterations in the function of large-conductance calcium- and voltage-activated potassium channels (BK_{Ca}, MaxiK, $K_{Ca}1.1$ or KCNMA1), a K^+ channel that co-localizes with caveolin in a cholesterol-rich membrane fraction and is implicated in cell signaling. The results are consistent with the hypothesis that 7-DHC contributes to SLOS pathogenesis, in part, by accumulating in the caveolar membrane where it disturbs membrane structure/function. However, additional findings of unanticipated complex ion channel activity along with alterations in Cav1 and BK_{Ca} mRNA and protein expression suggest that the human condition in which *DHCR7* mutations exist may be more complicated than mere alterations in 7-DHC and cholesterol levels.

Experimental Procedures

Reagents

The following lipids were obtained from Avanti Polar Lipids (Alabaster, AL) and used without further purification in these experiments: porcine brain L-α-*sn*-phosphatidylcholine (POPC), porcine brain sphingomyelin (SPM), and cholesterol (unesterified or free cholesterol, FC). 7-DHC and 8-dehydrocholesterol (8-DHC) were purchased from Sigma-Aldrich. Lipids were stored in chloroform at 10 mg/mL at −20°C until use.

Cell cultures of human SLOS skin fibroblasts

Skin fibroblasts were obtained from SLOS patients and healthy control subjects, and grown to confluence in MEM+10% fetal bovine serum (FBS) supplemented with nonessential amino acids. Prior to experiments, the SLOS cells were transferred to MEM+10% lipoprotein deficient serum (LPDS) for 5 – 7 days to remove exposure to exogenous cholesterol (lipoproteins) otherwise present in normal FBS. Fibroblasts from a total of 5 SLOS patients and 5 control subjects were used. All cells were studied between passage 4 and 11, and all assays were performed at 37°C. Approval to use human skin fibroblasts was granted by the University Institutional Review Boards prior to the initiation of this study.

Isolation of cholesterol-rich cell membrane fractions

Cholesterol-rich cell membrane fractions were isolated using a detergent-free method essentially as described by Song *et al.* [19]. Briefly, fibroblasts were scraped into 1 ml of 500 mM sodium carbonate, pH 11.0 and lysed by sheering through a 23-ga. needle 10 times

and sonicating 3 times for 15 seconds. The homogenate was adjusted to 40% sucrose and placed at the bottom of an ultracentrifuge tube. A 5–35% discontinuous sucrose gradient was applied above the homogenate by adding 6 ml of 35% sucrose and 4 ml of 5% sucrose (both in MBS containing 250 mM sodium carbonate) and centrifuged at 39,000 rpm for 3 hours in an SW41 rotor (Beckman Instruments, Palo Alto, CA). 1 mL fractions were aspirated starting from the top of the gradient. A light-scattering band confined to the 5–35% sucrose interface (*i.e.*, fraction 4), which contained caveolin (see Fig 4), was aspirated for further analysis.

Sterol analysis

For caveolar membrane sterol measurements, cholesterol-rich membrane fractions containing Cav-1 were isolated as described above. Coprostanol (1 mg) was added as an internal recovery standard and membrane pellets were extracted in chloroform/methanol/water [20]. The chloroform phase was collected and dried under nitrogen. Sterols were identified and quantitated using gas-liquid chromatography/mass spectrometry (GC/MS), as previously described [2]. Briefly, an aliquot of the extract was hydrolyzed in 1N NaOH ethanol for 1 hour at 70°C, extracted with *n*-hexane, and converted into trimethylsilyl (TMS) ether derivatives which were injected into a capillary column. This column was a chemically bonded, fused silica, nonpolar CP-Sil 5CB (25m × 0.25 mm ID: stationary phase, 100% dimethylsiloxane) (Chrompack, Raritan, NJ); helium was used as the carrier gas at a flow rate of 1 ml/min. To achieve optimal separation of sterols, the column oven temperature was programmed to change from 100°C to 265°C at 35°C/min after a 2 minute delay from the time of injection. The chromatograph was calibrated with a standard consisting of 1 μg each of authentic coprostanol and 7- and 8-DHC. Membrane sterol content was expressed as the ratio of sterol to protein. Protein was quantitated using the method of Lowry [21].

Preparation of model membranes

Model membrane vesicles were prepared from various combinations of palmitoyloleyl phosphatidylcholine (PC), sphingomyelin (SPM), free cholesterol (FC) and 7-DHC at molar ratios approximating those found in caveolar membrane fractions isolated from normal and SLOS skin fibroblasts [22–23]. For sterol location studies, “normal” (control) model membranes were prepared as ternary mixtures of PC:SPM:FC (3:1:2 mole ratio); “SLOS” model membranes were prepared as mixtures of PC:SPM:Sterol (3:1:2 mole ratio), with the sterol component made up of FC and 7-DHC at 1:1 mole ratio. For all membrane preparations, component lipids (in chloroform) were transferred to glass test tubes and shell-dried under nitrogen gas while vortex mixing. Residual solvent was removed by drying for a minimum of 1 hour under vacuum. After desiccation, each membrane sample was resuspended in diffraction buffer (0.5 mM HEPES, 154 mM NaCl, pH 7.3) to yield a final phospholipid concentration of 2.5 mg/mL. Multilamellar vesicles were then formed by vortex mixing for 3 min at ambient temperature [24].

Small Angle X-ray Diffraction Analyses

Lipid bilayers were oriented for x-ray diffraction analysis as previously described [25]. Briefly, 100 μL aliquots (containing 250 μg total phospholipid) of each multilamellar vesicle preparation were transferred to custom-designed Lucite® sedimentation cells, each containing an aluminum foil substrate upon which the final membrane sample pellets were collected. Samples were then loaded into a Sorvall AH-629 swinging bucket ultracentrifuge rotor (Dupont Corp., Wilmington, DE) and centrifuged at 35,000 *g* for 1 h at 5°C. Following orientation, the supernatants were aspirated and the aluminum foil substrates supporting the membrane pellets were removed from the sedimentation cells and mounted onto curved glass slides. The samples were then placed in hermetically sealed brass canisters in which temperature and relative humidity were regulated prior to and during x-ray diffraction

analyses. Saturated solutions of potassium tartrate ($K_2C_4H_4 \cdot ½H_2O$) were used to establish a relative humidity level of 74% in these experiments, and samples were incubated at this relative humidity for a minimum of 1 hour prior to experimental analysis.

The oriented membrane samples were aligned at grazing incidence with respect to a collimated, monochromatic x-ray beam (CuK_α radiation, $\lambda = 1.54$ Å) produced by a Rigaku Rotaflex RU-200, high-brilliance rotating anode microfocus generator (Rigaku-MSC, The Woodlands, TX). The fixed geometry beamline utilized a single Franks mirror providing nickel-filtered radiation ($K_{\alpha 1}$ and $K_{\alpha 2}$ unresolved) at the detection plane. Diffraction data were collected at 20°C on a one-dimensional, position-sensitive electronic detector (Hecus X-ray Systems, Graz, Austria) using a sample-to-detector distance of 150 mm. This technique allows for precise measurement of the unit cell periodicity or *d*-space of the membrane lipid bilayer which is defined as the distance from the center of one lipid bilayer to the next including surface hydration. The *d*-space for any given membrane multibilayer is calculated from Bragg's Law, $h\lambda = 2\, d \sin\theta$, where h is the diffraction order, λ is the wavelength of the x-ray radiation (1.54 Å), d is the membrane lipid bilayer unit cell periodicity and θ is the Bragg angle equal to one-half the angle between the incident beam and scattered beam. Fourier transformation of the collected x-ray diffraction data provides the time-averaged electron density distribution (distance in Å versus electrons/$Å^3$) across the membrane bilayer. Changes in electron density distribution that occur in the presence of an added component (such as 7-DHC) allow for the measurement of its time-averaged location in the bilayer. For location analyses, each individual diffraction peak was corrected using a linear subtraction routine that averaged background noise. The lamellar intensity functions from the oriented membrane samples were normalized by a factor of $s = \sin\theta/\lambda$, the Lorentz correction, and phases were assigned to each lamellar diffraction peak based on a swelling or hydration analysis, as previously described [26].

Electron Microscopy

SLOS and control skin fibroblasts were grown in 60 mm petri dishes. Cell cultures were fixed with 2.5% glutaraldehyde in 0.1 M sodium cacodylate, pH 7.4 for 30 min at room temperature. The cultures were later post-fixed with 1% osmium tetroxide in 0.1 M sodium cacodylate buffer, pH 7.4 for 1 hr, contrasted with 1% tannic acid in 0.05 M sodium cacodylate, followed by dehydration through graded alcohols and propylene oxide. During the propylene oxide step the cells were lifted off the dishes, transferred to microcentrifuge tubes and gently pelleted. Infiltration using graded epon solutions was performed and the cell pellets were embedded in EMbed 812 epon resin (Electron Microscopy Sciences, Hatfield, PA). Thin sections were cut on an UltraCut E ultramicrotome and stained with uranyl acetate and lead [27]}. Images were collected with an AMT XR41-B 4 megapixel camera on a Hitachi H-7000 electron microscope.

Immunoblot Analysis

For protein identification, the cells were washed with ice-cold Dulbecco's PBS and lysed in RIPA lysis buffer (150 mM NaCl, 1% Nonidet P-40, 1.0 mM EDTA and 50 mM Tris) containing 1 mM PMSF and 1X Protease Inhibitor Mixture™ (Roche Applied Science). For positive controls, thoracic aorta and whole brain were removed from 12–15 week old male Wistar-Kyoto (WKY) and spontaneously hypertensive rats (SHR, Charles River), cut into small pieces, and homogenized (Kontos glass homogenizer, Fisher Sci.) twice in cold lysis buffer of the following composition: 1X PBS, 1% Nonidet P40, 0.1% SDS, and 0.5% Na deoxycholate with protease (Complete mini, Roche Diagnostics) and phosphatase inhibitors (Halt, Pierce Biotechnology). Lysates from cells and tissue were centrifuged at 10,000 rpm (9800 × *g*) for 15 min at 4°C and the supernatant analyzed for protein content (BioRad protein assay, Hercules, CA) using albumin as a standard. Unless otherwise stated, equal

quantities of protein (30 μg) were separated by SDS-polyacrylamide gel electrophoresis (4–20% gradient gel), and electrophoretically transferred to nitrocellulose or polyvinylidene fluoride membranes. The blots were then probed with antibodies directed against BK_{Ca} (1:1000), caveolin-1 (1:2000), and β actin (1:10,000) (BD Transduction Laboratories). For two color detection, blots were incubated with both primary antibodies simultaneously, followed by IR-labeled secondary antibodies. Blots were imaged and quantitated on a Licor® Odyssey fluorescence imager in both 700 and 800 nm channels at 169 μm resolution.

mRNA Expression

RNA was isolated from cultured fibroblasts (RNAeasy, Qiagen) and first strand synthesis performed using random hexamer primers (Superscript Onestep, InVitrogen). The cDNAs were amplified by real time PCR (AB 7500) employing Cav-1 and BK_{Ca} -specific primers and fluorescently labeled probes (proprietary; obtained from Applied Biosystems). RNA expression was normalized to ribosomal 18s RNA.

Electrophysiology

Patch-clamp techniques were employed to measure BK_{Ca} currents in cell-attached or inside-out patches of human skin fibroblasts, as previously described [28]. Inside-out patches were examined in the presence of symmetrical 145 mM KCl, 1 mM $MgCl_2$, 10 mM glucose, 10 mM HEPES, pH 7.5 at room temperature. Recording pipettes (10–15 MΩ) were made from 1.2-mm borosilicate capillary glass using a Sutter P-84 puller (Sutter Instrument Co., Novato, CA). Voltage clamp protocols and data acquisition were controlled digitally by a PC interfaced to an A/D converter (Molecular Devices) using Clampex 8.0 (Axon Instruments, Foster City, CA). Data analysis was conducted using Clampfit 8.1 (Axon Instruments) and Origin 6.0 (Microcal Software Inc., Northhampton, MA). Steady-state channel activity was represented as the product of the number of channels in the bilayer during recording (N) and the open channel probability (P_o). N was determined by stepping voltage to positive levels to maximize P_o. NP_o values were determined from 1-minute duration measurements and defined as: $NP_o = \Sigma\,(t_1 + 2t_2 + 3t_3 + \ldots + nt_n)$, where N is channel number, P_o is open probability, and xt_x is the ratio of open time to total time of measurement for the channel at each current level. Unitary current amplitudes were determined by fitting the amplitude histogram to a Gaussian curve.

Genotyping

The fibroblasts cells lines were derived from subjects with SLOS. Genotyping was done on genomic DNA isolated from the buffy coats of these subjects (Gentra Systems, Minneapolis, MN). PCR products spanning all of the coding exons of *DHRC7* were sequenced, and the sequences were compared to the reference sequence in Gen Bank (Accession NC_00011).

Statistics

In all experiments, the number n equals the number of patients studied and the data are expressed as mean ± S.D. In most experiments, statistical analyses were performed on paired and unpaired data using either repeated measures analysis of variance (ANOVA) or the Students t-test. Multiple comparisons were analyzed using the Newman-Keuls post-hoc test. Statistical significance was defined as $P < 0.05$.

Results

Using skin fibroblasts obtained from SLOS patients, we isolated cholesterol-rich cell membranes, and analyzed them for sterol and caveolin. As shown in Fig. 2, cholesterol

content was 30% lower in the light membranes co-eluting with caveolin 1 (see also fraction 4, Fig. 4) isolated from SLOS patients compared to the same membrane fraction isolated from controls. 7-DHC, which was undetectable in controls, constituted approximately 35% of total sterol in the SLOS caveolar membranes. The total amount of sterol in SLOS caveolar membranes was approximately equal to that in control membranes. In addition, the concentration of cholesterol measured in control caveolar membranes (70±10 μg/mg protein) was almost 12-fold higher than that seen in non-caveolar plasma membrane fractions (5.9±2.7 μg/mg protein) isolated from human fibroblasts. These data are consistent with previous findings showing that cholesterol concentrates in the caveolar membrane and demonstrates that it is replaced by about one-third with 7-DHC in SLOS caveolae.

To assess the effect of 7-DHC on the structure and lipid organization of caveolar membranes, we used small angle x-ray diffraction approaches. Model membranes were prepared with PC, SM, FC and/or 7-DHC at ratios approximating those thought to occur in native caveolae [22–23]. Representative diffraction patterns, obtained from oriented control and SLOS-like model membranes, are shown in Fig. 3A. Four reproducible diffraction orders were obtained from both samples at 20°C with the most noticeable difference being the rightward shift of the diffraction peaks associated with 7-DHC-containing membranes (shaded peaks), an effect consistent with a decrease in *d*-space. *d*-space values largely reflect overall membrane width, i.e., from the lipid-aqueous phase interface on one side of the membrane to the lipid-aqueous phase interface of the opposing membrane leaflet [29–30]. The *d*-space value calculated for control membranes was 66.2 ±0.3Å; in the presence of 7-DHC, the membrane bilayer *d*-space decreased 4.8Å to 61.4 ± 0.3Å (7.3%). A change in bilayer width of 3–5 Å could affect a displacement of 2–4 amino acids, or nearly an entire turn of an α-helix (at 1.54 Å/amino acid) of a transmembrane protein. These data are consistent with the conclusion that the presence of 7-DHC in caveolar membranes at concentrations typically seen in SLOS cells likely decreases membrane width and may contribute to altered caveolar function.

Fourier transformation of the diffraction data yielded one-dimensional electron density profiles for control and 7-DHC-treated model membranes, as shown in Figure 3B. The electron density peaks on either side of the profile correspond to the electron-dense phospholipid headgroups; the minimum electron density at the center of the profile corresponds to the region occupied by the terminal methyl groups of the phospholipid acyl chains. The effects of 7-DHC on membrane structure were determined by subtracting the superimposed electron density profiles and are indicated by the horizontally oriented shaded areas in Figure 3B. 7-DHC treatment resulted in a discrete increase in electron density, and thus intermolecular packing in the hydrocarbon core region ± 0–11Å from the center of the membrane bilayer, consistent with its equilibrium location [7]. This type of alteration in a highly saturated membrane domain would be expected to increase lateral pressure impinging on membrane proteins spanning this region of the membrane. The decrease in *d*-space of 4.8Å calculated from the one-dimensional electron density profiles in figure 3A is confirmed as an inward shift in the electron density profile peaks relative to control (Fig. 3B). The same effect on membrane width was observed with an increase in 7-DHC content to 50% total sterol (data not shown).

In preliminary screening of membrane ion channel currents we found markedly altered single channel activity of large conductance, calcium-activated BK_{Ca} K^+ channels in SLOS fibroblasts. These channels are expressed in many mammalian cells, and are involved in regulating cell volume, membrane excitability, and signal transduction processes with important contribution to vital body functions, including vascular, renal, immune and neural activity [31]. Knockout of the gene coding for BK_{Ca} causes multiple organ malfunctions, for instance ataxia [32], progressive hearing loss [33], urinary bladder incontinence, and erectile

dysfunction [34], underscoring the important physiological role of BK_{Ca} channels. Recent reports in uterine myometrium [35–36] and arterial smooth muscle [34] have demonstrated that BK_{Ca} is contained in caveolae, and linked to and regulated by Cav-1. Moreover, altered caveolin-1 levels have been reported in SLOS lung parenchyma and have been suggested to result in caveolar-dependent signaling [37]. On the basis of this finding, we isolated membrane caveolae from fibroblasts using detergent-free methods and probed for BK_{Ca} and Cav-1 protein. Following isopycnic centrifugation, both BK_{Ca} and Cav-1 proteins were found to be colocalized in a membrane fraction that was highly enriched with cholesterol (Fig. 4). These results indicate that, like other tissues, BK_{Ca} channel proteins are associated with membrane caveolae in human skin fibroblasts.

In addition to the accumulation of 7DHC in the caveolar membrane and its likely effect on bilayer structure and dynamics, we also found an approximately 70% reduction in caveolin-1 protein in whole cell lystates of SLOS cells that was surprisingly associated with an even larger reduction (≈85%) in caveolin-1 mRNA levels (Fig. 5). The marked decrease in Cav-1 mRNA is consistent with down-regulation at the transcriptional level and decreased Cav-1 protein concentration. These findings combined with the accumulation of 7DHC in the caveolar membrane and its predicted changes in bilayer structure suggest possible alterations in caveolar number and/or structure in cells isolated from SLOS patients. Surprisingly, as shown in figure 6, typical flasked-shaped caveolae were readily observed within SLOS cells with no apparent differences in caveolar morphology as compared to control cells. In addition, a modest reduction in membrane-bound caveolae was detectable in only one of three SLOS cell lines evaluated.

Assessment of BK_{Ca} activity indicated that the function of BK_{Ca} channels was significantly altered in SLOS cells as illustrated in figure 7A. In addition to reduced whole cell currents, we found a pronounced rightward shift in the voltage dependence of channel open probability (Fig. 7B), which indicates that a much higher membrane voltage is necessary to activate BK_{Ca} currents in SLOS cells. The shift in $V_{½}$ of a Boltzmann's fit to the data averaged approximately 50 mV for all SLOS cells examined compared to normal healthy cells (Fig. 7C). These changes in BK_{Ca} channel activity may reflect alterations in BK_{Ca} −α subunit protein levels or in the molecular composition of BK_{Ca} channels in SLOS cells. Immunoblots of whole cell lysates of cells collected from SLOS and control patients revealed reduced BK_{Ca} protein levels in SLOS cells compared to controls (Fig. 8A). Rat brain and aortic lysates were included as positive controls. Slightly slower gel migration was observed for BK_{Ca} protein derived from rat tissue as compared to protein derived from human fibroblasts (dashed line in Fig. 8A), suggesting that the human form of BK_{Ca} may be a different splice variant or may be post-translationally modified compared to rat. On average, BK_{Ca} protein levels were reduced by approximately 80% in SLOS versus control cells (Fig. 8B). In contrast, there was no significant difference in BK_{Ca} mRNA levels between SLOS and control cells (Fig. 8C), The data thus raise the possibility of altered BK_{Ca} translation or altered protein stability.

Discussion

The primary objective of this study was to test the hypothesis that SLOS is associated with alterations in the sterol content of membrane caveolae and altered caveolar membrane structure and function. To this end, we found that 7-DHC, the immediate cholesterol precursor that accumulates in SLOS, replaces approximately 35% of the cholesterol content in the sterol- and caveolin-rich cell membrane fractions. Regarding the relative distribution of 7DHC, whole cell lystates contain approximately 8 μg 7DHC/mg protein and 33 μg FC/mg protein. Hence, <20% (41/8) of the total membrane sterol pool is comprised of 7DHC. Since we show in figure 2 that approximately 35% of the caveolar sterol pool is 7DHC, this

is consistent with the suggestion that 7DHC actually concentrates in the caveolar membrane. Associated with 7-DHC accumulation in membrane caveolae were subtle but potentially significant alterations in membrane structure and dynamics assessed in model membranes prepared to approximate the major lipid components of native caveolar membranes. These alterations included increased intermolecular packing within the hydrocarbon core of the membrane and an overall decrease in membrane width of approximately 7%. In addition, we found marked changes in the protein expression and functional properties of BK_{Ca}, an important modulator of cell signaling and cell function. Since this ion channel co-migrates with caveolin-1 in a membrane fraction highly enriched with cholesterol, has two consensus caveolin-binding motifs [34, 38–39] and is regulated, in part, by caveolin-1 [34–36], the data suggest a disrupting action of 7-DHC on caveolar membrane function. However, additional findings of complex alterations in BK_{Ca} conductance properties (e.g. shift in activation V½) along with a marked alteration in caveolin-1 transcription and translation, as well as BK_{Ca} translation without a change in mRNA levels indicate that additional and/or alternative mechanisms such as protein stability may underlie cellular derangements in SLOS cells. Hence we propose that the concept of an increase in 7-DHC, decrease in cholesterol, or a combination of the two as a primary basis of SLOS pathology is hard to defend.

To gain insights into how 7-DHC might interact with cholesterol and phospholipids in the caveolar membrane, we employed X-ray diffraction of model bilayers prepared to approximate the major lipid components of the caveolar membrane. We found that, unlike cholesterol which partitions into the glycerol backbone-hydrocarbon core interface region [40–41], 7-DHC intercalates deeper into the hydrocarbon core, 0–11 Å from the bilayer center. From this location, 7-DHC causes a 4.8Å (7.3%) decrease in membrane width and an increase intermolecular packing. These results suggest that similar changes may occur in membrane caveolae and call for experiments to confirm this suggestion using caveolae isolated from SLOS fibroblasts. In preliminary studies, we were not able to diffract native caveolar membranes to confirm these disturbances in SLOS cells. Nonetheless, our data demonstrate that the biophysical interactions of 7-DHC with membrane lipids are distinctly different from those of cholesterol and suggest that 7-DHC disturbs the lipid structural organization of membrane caveolae in SLOS. These findings are consistent with those of several other laboratories using a variety of different approaches to this question. For example, Rakheja and Boriack [42] demonstrated the accumulation of 7DHC in cholesterol-rich membrane domains prepared from an autopsy liver specimen of a SLOS infant. Consistent with this, Keller *et al.* [18] showed that 7-DHC and cholesterol were equally efficient at incorporating into lipid rafts in the brains of rats treated with the DHCR7 inhibitor AY9944, an agent that mimics the SLOS biochemical defect and phenotype in rats. However, in their study, gel electrophoresis analysis of raft fractions from AY9944-treated and control rats demonstrated multiple differences, all suggesting that 7-DHC perturbs raft protein content. Likewise, Shrivastava, et al., [13] have shown that 7-DHC markedly disturbs membrane organization and dynamics, whereas desmosterol, a cholesterol precursor in the Bloch cholesterol synthesis pathway does not. Like 7-DHC, desmosterol differs from cholesterol by a single double bond, but at carbon 24. This implies that the position of the double bond in the B ring of sterols is a major determinant in maintaining appropriate membrane order, dynamics and function as originally proposed by London's laboratory [43]. Other studies have shown that 7DHC forms raft domains in phospholipid bilayers so long as the phospholipids contained saturated fatty acyl chains [17, 44] but not when they contained unsaturated fatty acyl chains [17, 45]. Of note, the bilayers evaluated in our study were made up of POPC and sphingolipid, giving them an overall saturated hydrocarbon core region similar to native caveolar membranes [8]. It is important to point out that a criticism of studies in model membranes, including those used in this report, is that they never faithfully reflect the in vivo composition and dynamics of native cell membranes. Indeed, changes in other membrane lipids; e.g., phospholipids and fatty acyl chain characteristics are

often not taken into account. Nonetheless, Sanchez-Wandelmer *et al.*, [16] found negligible alterations in phospholipids in raft and non-raft membranes in 3T3-Li cells treated with the DHCR7 inhibitor AY9944, an often employed model of SLOS pathology. Thus we conclude that accumulation of 7-DHC in cell membranes, a hallmark of the SLOS metabolic phenotype, causes cell membrane structural abnormalities in vivo.

Interestingly, despite the changes in caveolar sterol composition and reduction in cav-1 protein levels, electron microscopic analysis of SLOS cells failed to show differences in the apparent quantity or morphology of plasma membrane-bound caveolae. On the contrary, typical flask-shaped caveolae were observed in relative abundance in cholesterol-free medium (LPDS). This observation is surprising since depletion of membrane cholesterol by extraction with cyclodextrins [35, 46–47], HMGCoA inhibition with statins [48–49], or silencing with siRNAs [36, 50] were all reported to alter membrane caveolae. Our observation of normal caveolae structure is consistent with the findings from London's laboratory [14, 43] that 7-DHC not only contributes to raft formation in model membranes, but does so even better than cholesterol. However, as suggested by our data and that of others [12–13, 17–18, 43], the ability of 7DHC to participate in the formation of raft-like domains does not exclude a negative impact of 7-DHC on caveolae function.

As a measure of caveolar "function", we selected the large conductance voltage and calcium-activated BK_{Ca} K^+ channel to study because it possesses at least two cav-1 binding motifs [38–39] and has been shown to be a caveolin bound and caveolin regulated protein in other cell types [35–36, 51] including fibroblasts [36], and its activity has been shown to be sensitive to changes in membrane lipid dynamics secondary to 7DHC inclusion [52]. While screening membrane currents that might be altered in SLOS cells, we found this channel to be markedly altered compared to control cells. Like others [31, 35, 53], we show that BK_{Ca} localizes to a membrane fraction enriched with both cholesterol and caveolin (Fig. 4). Caveolar membranes have characteristics that are distinct from those of non-caveolar membranes, including increased bilayer width and lipid structural order [8], properties that are essential for the normal function of resident proteins [54]. Changes in caveolar membrane width, lipid order or lateral pressure would be expected to alter the conformation and function of associated transmembrane proteins. For example, in model membranes of varying thicknesses, BK_{Ca} channel activity was shown to be directly affected by bilayer thickness [52, 55], primarily by affecting the stability of the closed state. X-ray diffraction data collected in the present study suggest that 7-DHC may affect BK_{Ca} function by altering caveolar bilayer width and lipid structural organization. Accordingly, we assessed BK_{Ca} channel activity. Using single channel patch recording techniques, we discovered that BK_{Ca} channels are present in both normal (control) and SLOS fibroblasts. However, BK_{Ca} activity is grossly altered in SLOS cells as reflected by a reduced single channel conductance (Fig 7A) and a 50 mV shift in the half-maximal voltage required to activate channel opening (Fig. 7B). Supporting a membrane role in mediating at least some of these abnormalities in BK_{Ca} activity, enrichment of caveolar membranes with sterols has been shown to produce qualitatively similar results as seen in the present study, i.e., a rightward shift in the activation voltage of Kv1.5, an unrelated voltage-activated K^+ channel [56]. Similar findings have been reported on the effects of experimentally altered membrane cholesterol levels on activation and inactivation properties of caveolar ion channels emphasizing the importance of appropriate sterol content on caveolar function [57–60]. It is of interest however, that Singh, et al., [12] found that adding 7-DHC to model bilayers containing the $5HT_{1A}$ receptor altered both lateral membrane pressure and 5HT binding. Changes in lateral pressure are known to alter the conformation of nearby membrane proteins, and this effect may explain the alterations in the BK_{Ca} activity observed in this study. These observations notwithstanding, additional studies are necessary to rule out other contributing factors such as altered expression of BK_{Ca} α-subunit splice variants, altered association with β_1 subunits,

and/or disturbances in the association of BK_{Ca} channels with its numerous signaling partners. However, a lipid bilayer-BK_{Ca} protein mismatch is not unreasonable, and is consistent with the concept of defective caveolar signaling in SLOS. Support for this conclusion comes from a study by Kovorova, et al., [61] who showed accumulation of 7-DHC in lipid rafts isolated from mast cells obtained from a *Dhcr7* knockout mouse model of SLOS. In their study, altered mast cell raft sterols were associated with hyperresponsiveness to degranulation following raft-associated IgE stimulation, consistent with raft dysregulation cause by 7DHC accumulation in the raft membrane.

Our finding of reduced BK_{Ca} protein in SLOS cells was unanticipated and a mechanism based on 7DHC accumulation is not clear. One possibility is that 7-DHC accumulates in the endoplasmic reticulum (ER) membrane where its accumulation might impair the sensing of missfolded proteins and thus lead to a posttranslational clearing of BK_{Ca} through the endoplasmic reticulum protein degradation (ERAD) pathway. Of note, Fitzky, et al., [62] found a decrease in HMGCoA reductase protein in fibroblasts isolated from the *Dhcr7* knockout mouse mediated by an apparent action of 7-DHC on the ER membrane. Likewise open for speculation was the unanticipated reduction in caveolin-1 mRNA levels in the SLOS cells. It is speculated that 7-DHC accumulation in the ER membrane may upregulate the sterol regulatory element binding protein (SREBP), which can bind to sterol regulatory elements in the Cav-1 promoter [63] and thus inhibit Cav-1 transcription and mRNA levels. However, the degree to which 7-DHC might interact with this SRE, and how, has not been studied, but an explanation based on dysregulation at the level of the Cav-1 promoter SRE is plausible.

In conclusion, our data are consistent with the hypothesis that caveolar membrane alterations are secondary to accumulation of 7-DHC in SLOS cells and significantly impair cell signaling. Due to the ubiquitous presence of caveolae in all cells of the body, such alterations could account for some of the phenotypic features in SLOS patients. Confirmation of this hypothesis will require further studies where, for example, correction of the genetic anomaly restores the SLOS membrane phenotype.

Acknowledgments

The authors wish to thank Francine G. Hanley and Terrance Z. Kirk for their expert assistance with this study. We also thank Dr. Amit Chattopadhyay for critically reviewing the manuscript and providing comments. Support for this project was provided in part by NIH grants R01-HD-40284, R01-HL-66273 (TNT), R01-HL-73980 (RDS), R01-HL-28476 (RHC) and the Office of Research and Development, Medical Research Service, Department of Veterans Affairs (GST). The authors also wish to acknowledge Yong-Feng Yang PhD at the OHSU OCHRC Tissue Culture Core supported by K12 HD-33703 for expert technical assistance, and Jennifer Penfield, MS, for expert patient care.

References

1. Salen G, Shefer S, Batta A, Tint G, Xu G, Honda A, Irons M, Elias E. Abnormal cholesterol biosynthesis in the Smith-Lemli-Opitz syndrome. J Lipid Res. 1996; 37:1169–1180. [PubMed: 8808751]
2. Tint GS, Irons M, Elias ER, Batta AK, Frieden R, Chen TS, Salen G. Defective cholesterol biosynthesis associated with the Smith-Lemli-Opitz syndrome. N Engl J Med. 1994; 330:107–113. [PubMed: 8259166]
3. Correa-Cerro LS, Porter FD. 3b-hydroxysterol D7-reductase and the Smith-Lemli-Optiz syndrome. Mol. Genet Metab. 2005; 84:112–126. [PubMed: 15670717]
4. Yu H, Patel S. Recent insights into the Smith-Lemli-Opitz syndrome. Clin Genet. 2005; 68:383–391. [PubMed: 16207203]
5. Honda A, Tint GS, Salen G, Kelley RI, Honda M, Batta AK, Chen TS, Shefer S. Sterol concentrations in cultured Smith-Lemli-Opitz syndrome skin fibroblasts: diagnosis of a

biochemically atypical case of the syndrome. Am J Med Genet. 1997; 68:282–287. [PubMed: 9024560]

6. Wassif C, Vied D, Tsokos M, Connor W, Steiner R, Porter F. Cholesterol storage defect in RSH/Smith-Lemli-Opitz syndrome fibroblasts. Mol Genet Metab. 2002; 75:325–334. [PubMed: 12051964]
7. Tulenko TN, Boeze-Battaglia K, Mason RP, Tint GS, Steiner RD, Connor WE, Labelle EF. A membrane defect in the pathogenesis of the Smith-Lemli-Opitz syndrome. J. Lipid Res. 2006; 147:134–143. [PubMed: 16258167]
8. Simons K, Ikonen E. Functional rafts in cell membranes. Nature. 1997; 387:569–572. [PubMed: 9177342]
9. Rothberg K, Heuser J, Donzell W, Ying Y, Glenney J, RG A. Caveolin, a protein component of caveolae membrane coats. Cell. 1992; 68:673–682. [PubMed: 1739974]
10. Pol A, Martin S, Fernández M, Ingelmo-Torres M, Ferguson C, Enrich C, Parton R. Cholesterol and fatty acids regulate dynamic caveolin trafficking through the Golgi complex and between the cell surface and lipid bodies. Mol Biol Cell. 2005; 16:2091–2105. [PubMed: 15689493]
11. Thomas C, Smart E. Caveolae structure and function. J Cell Mol Med. 2008; 12:796–809. [PubMed: 18315571]
12. Singh P, Paila Y, Chattopadhyay A. Differential effects of cholesterol and 7-dehydrocholesterol on the ligand binding activity of the hippocampal serotonin(1A) receptor: implications in SLOS. Biochem Biophys Res Commun. 2007; 358:495–499. [PubMed: 17493586]
13. Shrivastava S, Paila Y, Dutta A, Chattopadhyay A. Differential effects of cholesterol and its immediate biosynthetic precursors on membrane organization. Biochemistry. 2008; 47:5668–5677. [PubMed: 18442257]
14. Megha Bakht O, London E. Cholesterol precursors stabilize ordinary and ceramide-rich ordered lipid domains (lipid rafts) to different degrees. Implications for the Bloch hypothesis and sterol biosynthesis disorders. J. Biol. Chem. 2006; 281:21903–21913. [PubMed: 16735517]
15. Samuli Ollila OH, Rog T, Karttunen M, Vattulainen I. Role of sterol type on lateral pressure profiles of lipid membranes affecting membrane protein functionality: comparison between cholesterol, desmosterol, 7-dehydrocholesterol and ketosterol. J. Struct. Biol. 2007; 159:311–323. [PubMed: 17369050]
16. Sánchez-Wandelmer J, Dávalos A, Herrera E, Giera M, Cano S, de la Peña G, Lasunción M, Busto R. Inhibition of cholesterol biosynthesis disrupts lipid raft/caveolae and affects insulin receptor activation in 3T3-L1 preadipocytes. Biochim Biophys Acta. 2009; 1788:1731–1739. [PubMed: 19433058]
17. Jansen M, Pietiäinen V, Pölönen H, Rasilainen L, Koivusalo M, Ruotsalainen U, Jokitalo E, Ikonen E. Cholesterol substitution increases the structural heterogeneity of caveolae. J. Biol. Chem. 2008; 283:14610–14618. [PubMed: 18353778]
18. Keller R, Arnold T, Fliesler S. Formation of 7-dehydrocholesterol-containing membrane rafts in vitro and in vivo, with relevance to the Smith-Lemli-Opitz syndrome. J Lipid Res. 2004; 45:347–355. [PubMed: 14594996]
19. Song K, Shengwen L, Okamoto T, Quilliam LA, Sargiacomo M, Lisanti MP. Co-purification and direct interaction of Ras with caveolin, an integral membrane protein of caveolae microdomains. Detergent-free purification of caveolae microdomains. J Biol Chem. 1996; 271:9690–9697. [PubMed: 8621645]
20. Bligh EG, Dyer WJ. A rapid method of total lipid extraction and purification. Can J Biochem. 1959; 37:911–917. [PubMed: 13671378]
21. Lowry OH, Rosenbrough NJ, Farr AL, Randall RJ. Protein measurement with the folin phenol reagent. J Biol Chem. 1951; 193:265–275. [PubMed: 14907713]
22. Pike L. Lipid rafts: bringing order to chaos. J Lipid Res. 2003; 44:655–667. [PubMed: 12562849]
23. Pike L, Han X, Chung K, Gross R. Lipid rafts are enriched in arachidonic acid and plasmenylethanolamine and their composition is independent of caveolin-1 expression: a quantitative electrospray ionization/mass spectrometric analysis. Biochemistry. 2002; 41:2075–2088. [PubMed: 11827555]

24. Bangham A, Standish M, Watkins J. Diffusion of univalent ions across the lamellae of swollen phospholipids. J Mol Biol. 1965; 13:238–252. [PubMed: 5859039]
25. Herbette L, DeFoor P, Fleischer S, Pascolini D, Scarpa A, Blasie J. The separate profile structures of the functional calcium pump protein and the phospholipid bilayer within isolated sarcoplasmic reticulum membranes determined by X-ray and neutron diffraction. Biochim Biophys Acta. 1985; 817:103–122. [PubMed: 3159429]
26. Moody M. X-ray diffraction pattern of nerve myelin: a method for determining the phases. Science. 1963; 142:1173–1174. [PubMed: 14069237]
27. Sato T. A modified method for lead staining of thin sections. J. Electron Microsc. 1968; 17:158–159.
28. Cox R, Lozinskaya I, Dietz NJ. Calcium exerts a larger regulatory effect on potassium channels in small mesenteric artery mycoytes from spontaneously hypertensive rats compared to Wistar-Kyoto rats. Am J Hypertens. 2003; 16:21–27. [PubMed: 12517678]
29. Chen M, Mason RP, Tulenko TN. Atherosclerosis alters composition, structure and function of arterial smooth muscle plasma membranes. Biochim. Biophys. Acta. 1995; 1272:101–112. [PubMed: 7548233]
30. Tulenko TN, Chen M, Mason PE, Mason RP. Physical effects of cholesterol on arterial smooth muscle membranes: Evidence of immiscible cholesterol domains and alterations in bilayer width during atherogenesis. J. Lipid Res. 1998; 39:947–956. [PubMed: 9610760]
31. Lu R, Alioua A, Kumar Y, Eghbal iM, Stefani E, Toro L. MaxiK channel partners: physiological impact. J Physiol. 2006; 570:65–72. [PubMed: 16239267]
32. Sausbier M, et al. Cerebellar ataxia and Purkinje cell dysfunction caused by Ca^{2+}-activated K^+ channel deficiency. Proc Natl Acad Sci U S A. 2004; 101:9474–9478. [PubMed: 15194823]
33. Ruttiger L, Sausbier M, Zimmermann U, Winter H, Braig C, Engel J, Knirsch M, Arntz C, Langer P, Hirt B, Muller M, Kopschall I, Pfister M, Munkner S, Rohbock K, Pfaff I, Rusch A, Ruth P, Knipper M. Deletion of the Ca2+-activated potassium (BK) alpha-subunit but not the BKbeta1-subunit leads to progressive hearing loss. Proc Natl Acad Sci U S A. 2004; 101:12922–12927. [PubMed: 15328414]
34. Alioua A, Lu R, Kumar Y, Eghbali M, Kundu P, Toro L, Stefani E. Slo1 Caveolin-binding Motif, a Mechanism of Caveolin-1-Slo1 Interaction Regulating Slo1 Surface Expression. J Biol Chem. 2008; 283:4808–4817. [PubMed: 18079116]
35. Brainard A, Miller AJ, Martens JR, England SK. Maxi-K channels localize to caveolae in human myometrium: a role for an actin-channel-caveolin complex in the regulation of myometrial smooth muscle K^+ current. Am J Physiol Cell Physiol. 2005; 289:C49–C57. [PubMed: 15703204]
36. Brainard A, Korovkina V, England S. Disruption of the maxi-K-caveolin-1 interaction alters current expression in human myometrial cells. Reprod Biol Endocrinol. 2009; 7:1–10. [PubMed: 19133142]
37. Katheria A, Masliah E, Benirschke K, Jones K, Kim J. Idiopathic persistent pulmonary hypertension in an infant with Smith-Lemli-Opitz syndrome. Fetal Pediatr Pathol. 2010; 29:373–379. [PubMed: 21043560]
38. Couet J, Li S, Okamoto T, Ikezu T, Lisanti M. Identification of peptide and protein ligands for the caveolin-scaffolding domain. Implications for the interaction of caveolin with caveolae-associated proteins. J Biol Chem. 1997; 272:6525–6533. [PubMed: 9045678]
39. Wang Y, Yamaguchi K, Wada T, Hata K, Zhao X, Fujimoto T, Miyagi T. A close association of the ganglioside-specific sialidase Neu3 with caveolin in membrane microdomains. J Biol Chem. 2002; 277:26252–26259. [PubMed: 12011038]
40. McIntosh T. The effect of cholesterol on the structure of phosphatidylcholine bilayers. Biochim Biophys Acta. 1978; 513:43–58. [PubMed: 718889]
41. Yeagle P. Cholesterol and the cell membrane. Biochim Biophys Acta. 1985; 822:267–287. [PubMed: 3904832]
42. Rakheja D, Boriack R. Precholesterol sterols accumulate in lipid rafts of patients with Smith-Lemli-Opitz syndrome and X-linked dominant chondrodysplasia punctata. Pediatr Dev Pathol. 2008; 11:128–132. [PubMed: 17378665]

43. Xu X, Bittman R, Duportail G, Heissler D, Vilcheze C, London E. Effect of the structure of natural lipids and sphingolipids on the formation of ordered sphingolipid/sterol domains (rafts). J. Biol. Chem. 2001; 276:33540–33546. [PubMed: 11432870]
44. Berring E, Borrenpohl K, Fliesler S, Serfis A. A comparison of the behavior of cholesterol and selected derivatives in mixed sterol-phospholipid Langmuir monolayers: a fluorescence microscopy study. Chem Phys Lipids. 2005; 136:1–12. [PubMed: 15904906]
45. Serfis A, Brancato S, Fliesler S. Comparative behavior of sterols in phosphatidylcholine-sterol monolayer films. Biochim Biophys Acta. 2001; 1511:341–348. [PubMed: 11286977]
46. Gustavsson J, Parpal S, Karlsson M, Ramsing C, Thorn H, Borg M, Lindroth M, Peterson K, Magnusson K, Strâlfors P. Localization of the insulin receptor in caveolae of adipocyte plasma membrane. FASEB J. 1999; 13:1961–1971. [PubMed: 10544179]
47. Parpal S, Karlsson M, Thorn H, Strålfors P. Cholesterol depletion disrupts caveolae and insulin receptor signaling for metabolic control via insulin receptor substrate-1, but not for mitogen-activated protein kinase control. J Biol Chem. 2001; 276:9670–9678. [PubMed: 11121405]
48. Zhuang L, Kim J, Adam R, Solomon K, Freeman M. Cholesterol targeting alters lipid raft composition and cell survival in prostate cancer cells and xenografts. J Clin Invest. 2005; 115:959–968. [PubMed: 15776112]
49. Jury E, Isenberg D, Mauri C, Ehrenstein M. Atorvastatin restores Lck expression and lipid raft-associated signaling in T cells from patients with systemic lupus erythematosus. J Immunol. 2006; 177:7416–7422. [PubMed: 17082661]
50. Amberg G, Bonev A, Rossow C, Nelson M, Santana L. Modulation of the molecular composition of large conductance, Ca^{2+} activated K^+ channels in vascular smooth muscle during hypertension. J Clin Invest. 2003; 112:717–724. [PubMed: 12952920]
51. Shmygol A, Noble K, Wray S. Depletion of membrane cholesterol eliminates the Ca^{2+}-activated component of outward potassium current and decreases membrane capacitance in rat uterine myocytes. J Physiol. 2007; 581:445–445. [PubMed: 17331986]
52. Yuan C, O'Connell RJ, Jacob RF, Mason RP, Treistman S. Regulation of the gating of BKCa channel by lipid bilayer thickness. J Biol Chem. 2007; 282:7276–7286. [PubMed: 17209047]
53. Wang X, Ye D, Peterson T, Cao S, Shah V, Katusic Z, Sieck G, Lee H. Caveolae targeting and regulation of large conductance Ca(2+)-activated K^+ channels in vascular endothelial cells. J Biol Chem. 2005; 280:11656–11664. [PubMed: 15665381]
54. Lee A. Cell biology: a greasy grip. Nature. 2005; 438:569–570. [PubMed: 16319869]
55. Yuan C, O'Connell R, Wilson A, Pietrzykowski A, Treistman S. Acute alcohol tolerance is intrinsic to the BKCa protein, but is modulated by the lipid environment. J Biol Chem. 2008; 283:5090–5098. [PubMed: 18084004]
56. McEwen D, Li Q, Jackson S, Jenkins P, Martens J. Caveolin regulates kv1.5 trafficking to cholesterol-rich membrane microdomains. Mol Pharmacol. 2008; 73:678–685. [PubMed: 18045854]
57. Maguy A, Hebert T, Nattel S. Involvement of lipid rafts and caveolae in cardiac ion channel function. Cardiovasc Res. 2006; 69:798–807. [PubMed: 16405931]
58. Martens J, O'Connell K, Tamkun M. Targeting of ion channels to membrane microdomains: localization of KV channels to lipid rafts. Trends Pharmacol Sci. 2004; 25:16–21. [PubMed: 14723974]
59. Pottosin I, Valencia-Cruz G, Bonales-Alatorre E, Shabala S, Dobrovinskaya O. Methyl-beta-cyclodextrin reversibly alters the gating of lipid rafts associated Kv1.3 channels in Jurkat T lymphocytes. Pflugers Arch. 2007; 454:235–244. [PubMed: 17242956]
60. Barbuti A, Gravante B, Riolfo M, Milanesi R, Terragni B, D D. Localization of pacemaker channels in lipid rafts regulates channel kinetics. Circ Res. 2004; 94:1325–1331. [PubMed: 15073040]
61. Kovarova M, Wassif C, Odom S, Liao K, Porter F, Rivera J. Cholesterol deficiency in a mouse model of Smith-Lemli-Opitz syndrome reveals increased mast cell responsiveness. J Exp Med. 2006; 203:1161–1171. [PubMed: 16618793]
62. Fitzky B, Moebius FF, Asaoka H, Waage-Baudet H, Xu L, Xu G, Maeda N, Kluckman K, Hiller S, Yu H, Batta AK, Shefer S, Chen T, Salen G, Sulik K, Simoni RD, Ness GC, Glossmann H, Patel

SB, Tint GS. 7-Dehydrocholesterol-dependent proteolysis of HMG-CoA reductase suppresses sterol biosynthesis in a mouse model of Smith-Lemli-Opitz/RSH syndrome. J Clin Invest. 2001; 108:905–915. [PubMed: 11560960]

63. Bist A, Fielding PE, Fielding CJ. Two sterol regulatory element-like sequences mediate up-regulation of caveolin gene transcription in response to low density lipoprotein free cholesterol. PNAS. 1997; 94:10693–10698. [PubMed: 9380697]

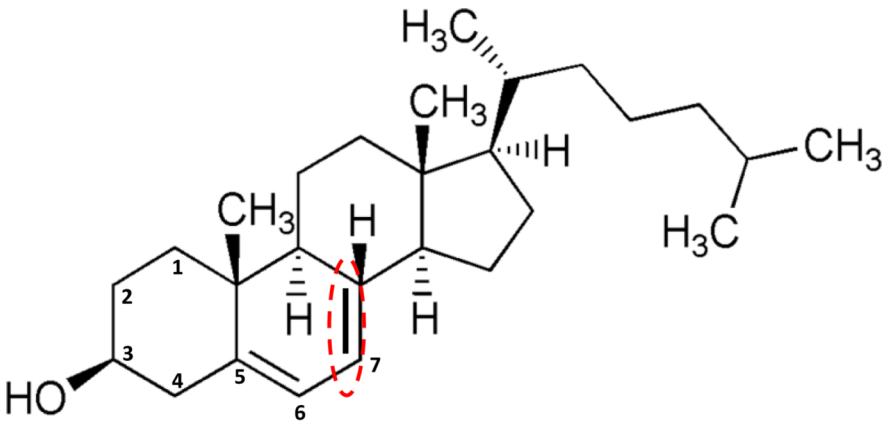

7-dehydrocholesterol

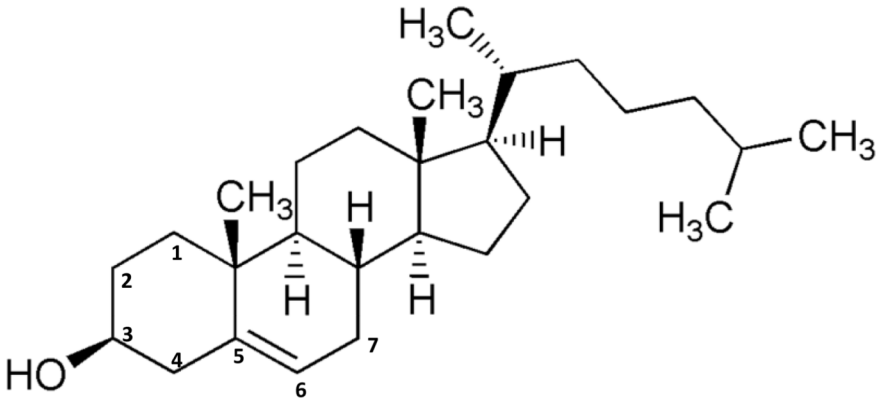

Cholesterol

Figure 1. Chemical structures of cholesterol and 7-dehydrochlesterol (7-DHC)
Note that the only difference between the two molecules is the presence of a double bond between carbons 7 and 8 in 7-DHC.

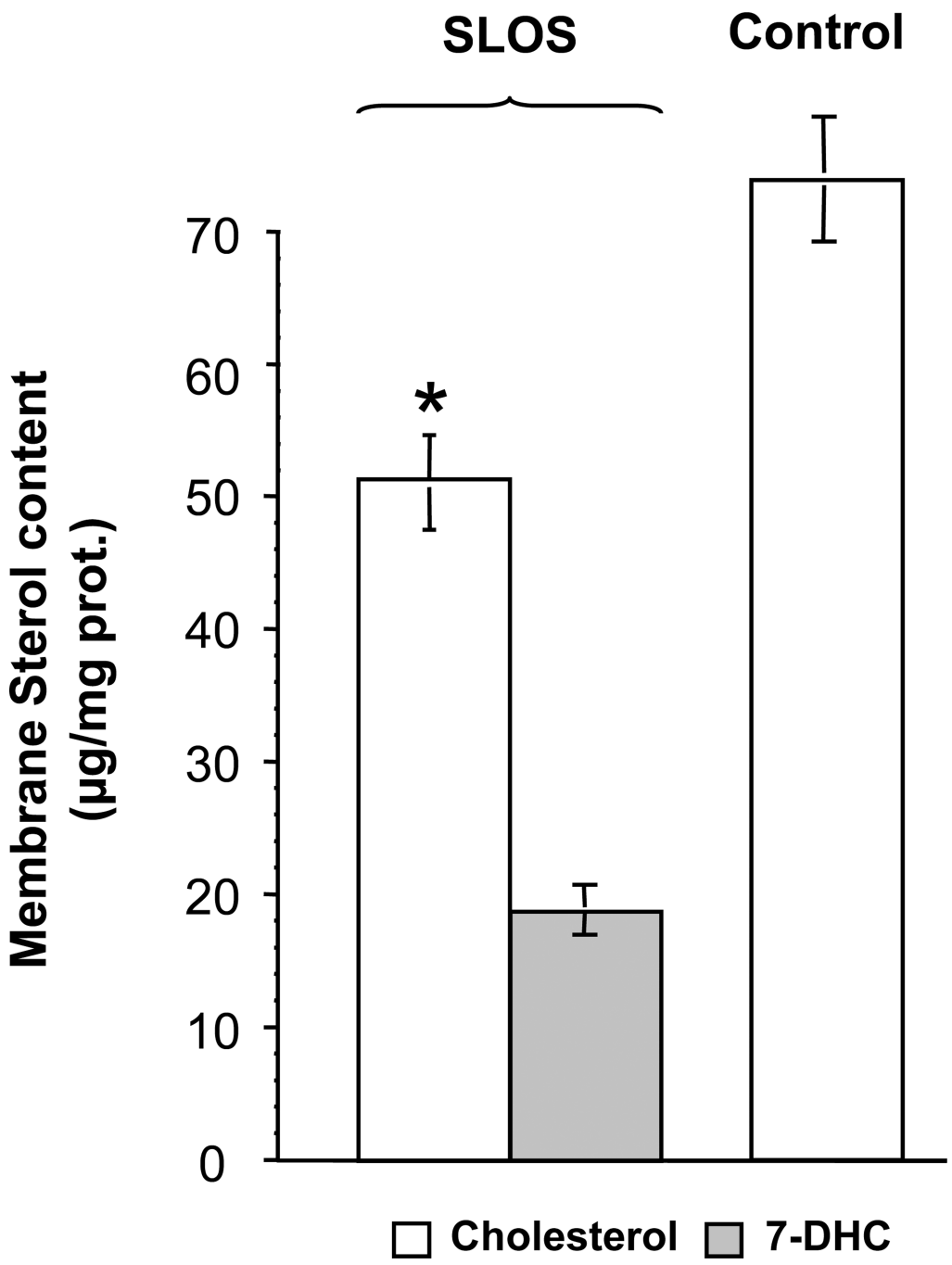

Figure 2. Altered sterol content of caveolin-rich membranes in SLOS fibroblasts

Sterols were measured in caveolin-rich membrane fractions (see fraction 4, Fig. 4) by GC/MS. Cholesterol and 7-DHC are represented by open and solid bars, respectively, demonstrating that 7-DHC replaces about a third of the cholesterol in the caveolar membranes isolated from SLOS patients. *$p < 0.01$, control (n=5 patients) vs. SLOS (N=6 patients).

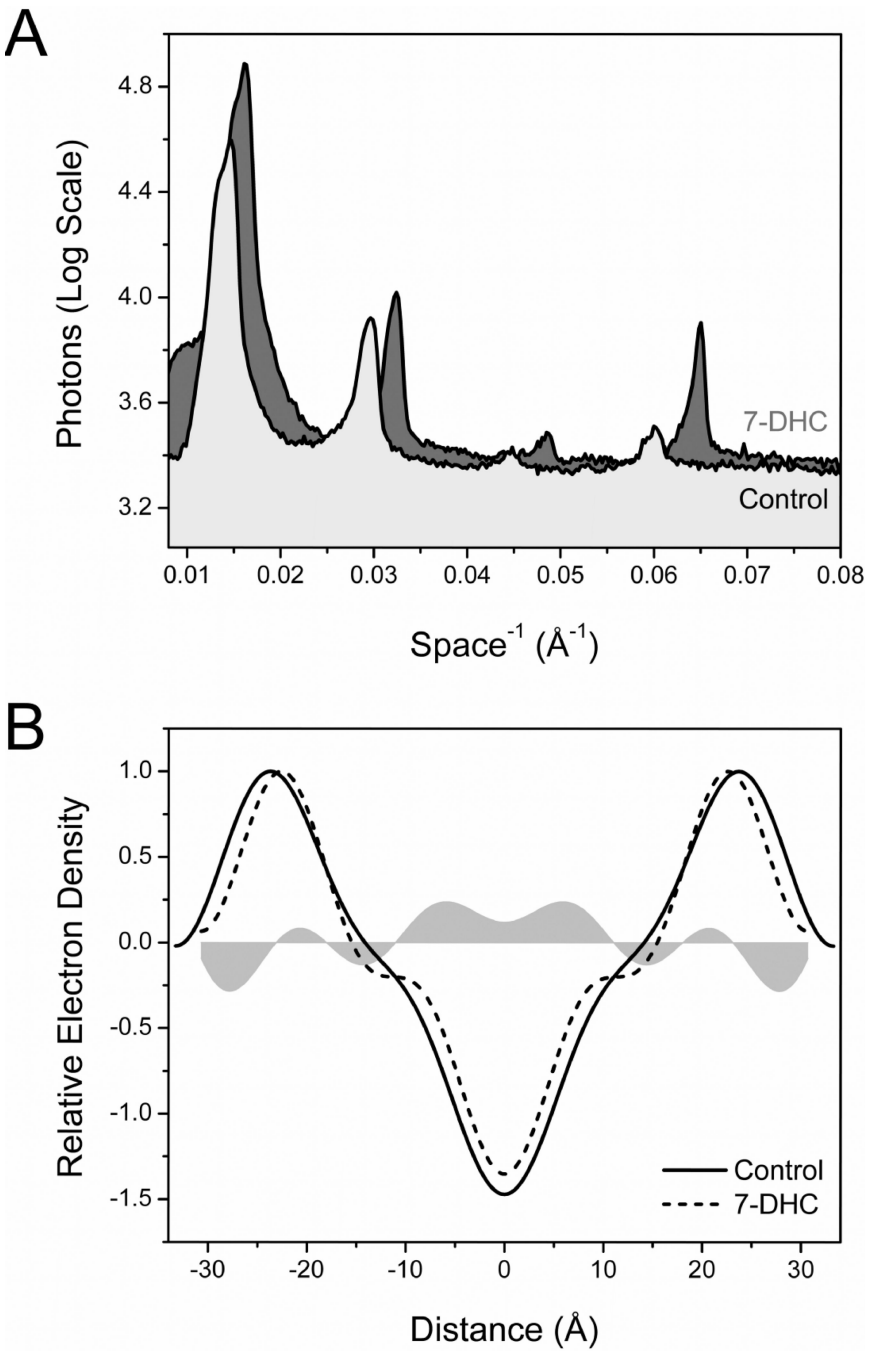

Figure 3. Altered membrane structure in model caveolar membranes

(A) Representative x-ray diffraction patterns collected from control and 7-DHC rich model membranes. The diffraction peaks associated with the 7-DHC-containing sample are shifted to the right relative to control, an effect consistent with a decrease in membrane bilayer width. (B) Electron density profiles across the membrane bilayer for control (solid line) and SLOS-like membranes (dashed line) are superimposed. The shaded area represents differences in electron density between control and 7-DHC-treated samples and was calculated by direct subtraction of their representative profiles. These data indicate that 7-DHC intercalates into the hydrocarbon core region, as evidenced by a broad increase in electron density, 0–11 Å from the center of the membrane bilayer.

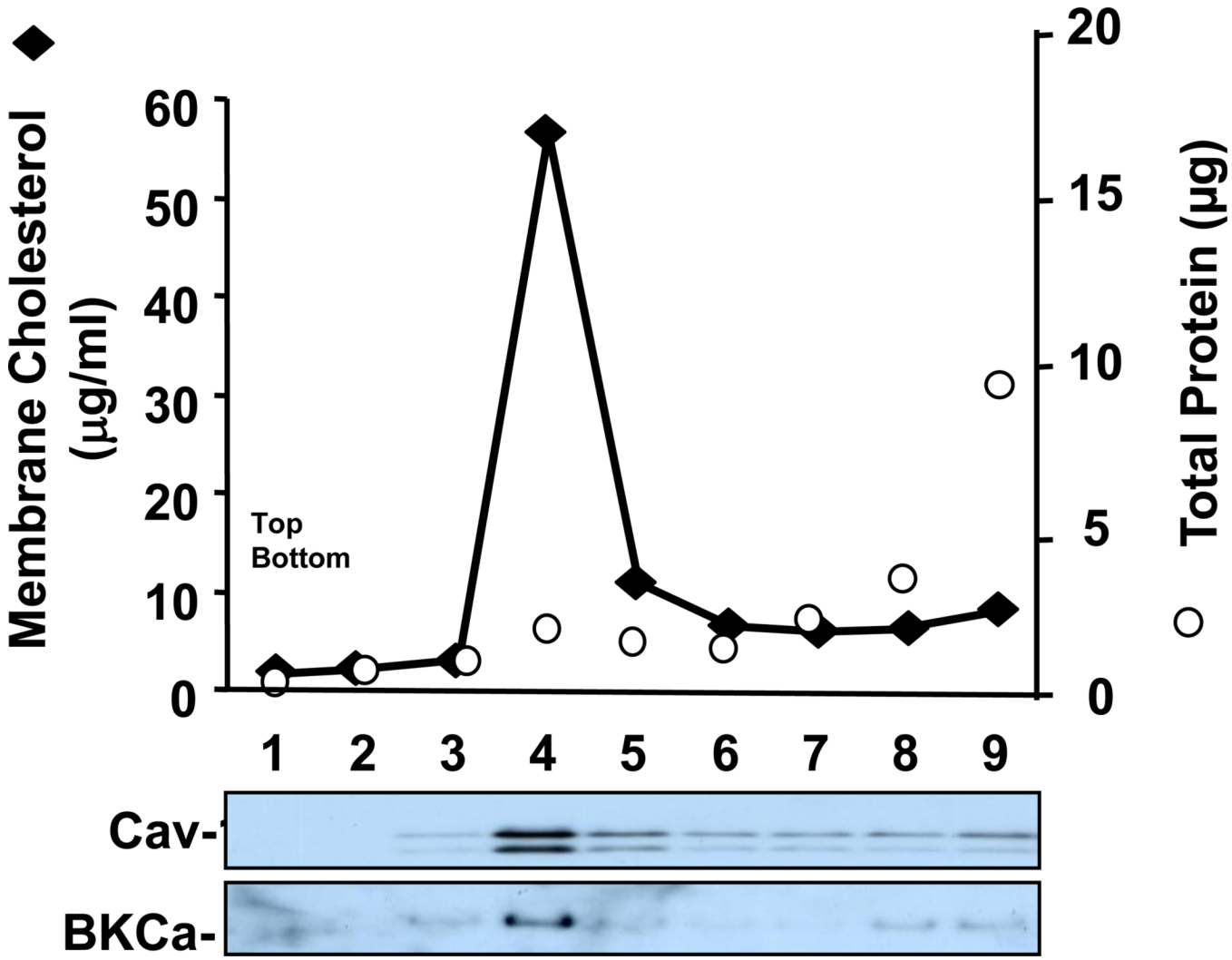

Figure 4. BK_{Ca} migrates with caveolin-1 and a cholesterol-rich membrane fraction

Separation of cellular membranes by isopycnic sucrose density ultracentrifugation demonstrates Cav-1 co-migration with cholesterol and BK_{Ca}. Membrane fractions were isolated from cell lysates spun on a discontinuous sucrose gradient and 1 mL fractions were collected for analysis from the top to bottom of the gradient. The cholesterol-rich fraction (fraction 4) was subjected to GC/MS analysis and reported in figure 2.

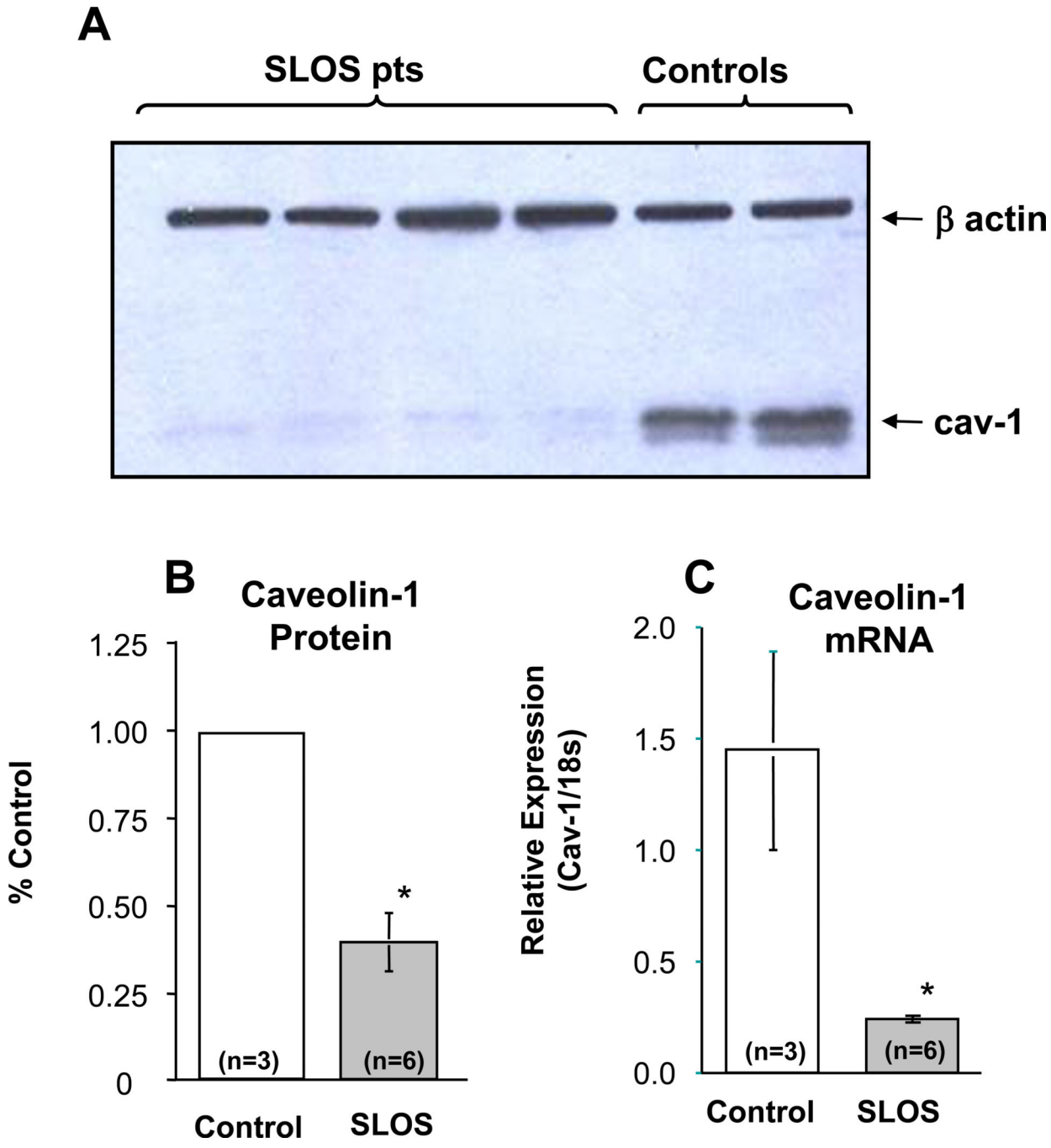

Figure 5. Caveolin-1 protein and mRNA expression in SLOS cells

(A) Immunoblot of caveolin-1 protein in control and SLOS fibroblasts suggest a marked decrease in caveolin-1 protein in SLOS cells. β actin is included as a loading control. (B) Quantitation of caveolin-1 in control and SLOS cells confirms an average decrease of over 60% in caveolin-1 protein in SLOS cells. (C) However, caveolin-1 mRNA levels in control and SLOS cells as determined by qPCR demonstrate a decrease in caveolin-1 mRNA levels in SLOS cells of approximately 80%. n = numbers of patients studied; *$p \leq 0.01$.

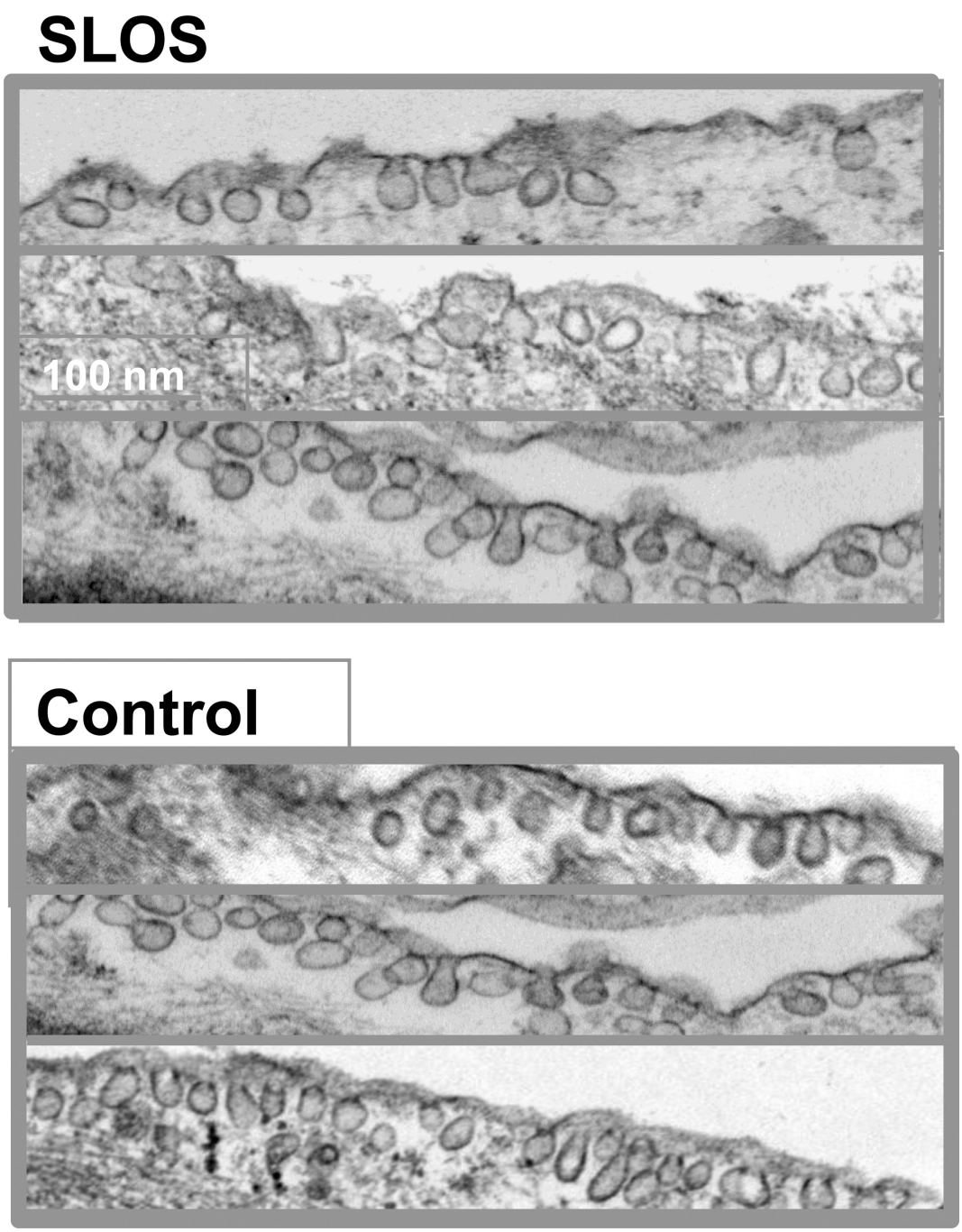

Figure 6. Membrane caveolae in SLOS cells

Electron micrographs from SLOS (top) and healthy control (bottom) fibroblasts clearly show numerous well-formed membrane caveolae in SLOS cells, despite the presence of 7DHC and reduction in caveolin-1 protein in these cells. Each frame is an image photographed from a different control (n=2) or SLOS (n=3) cell line, and is representative of 10–16 images taken for each sample. Bar = 250 μ

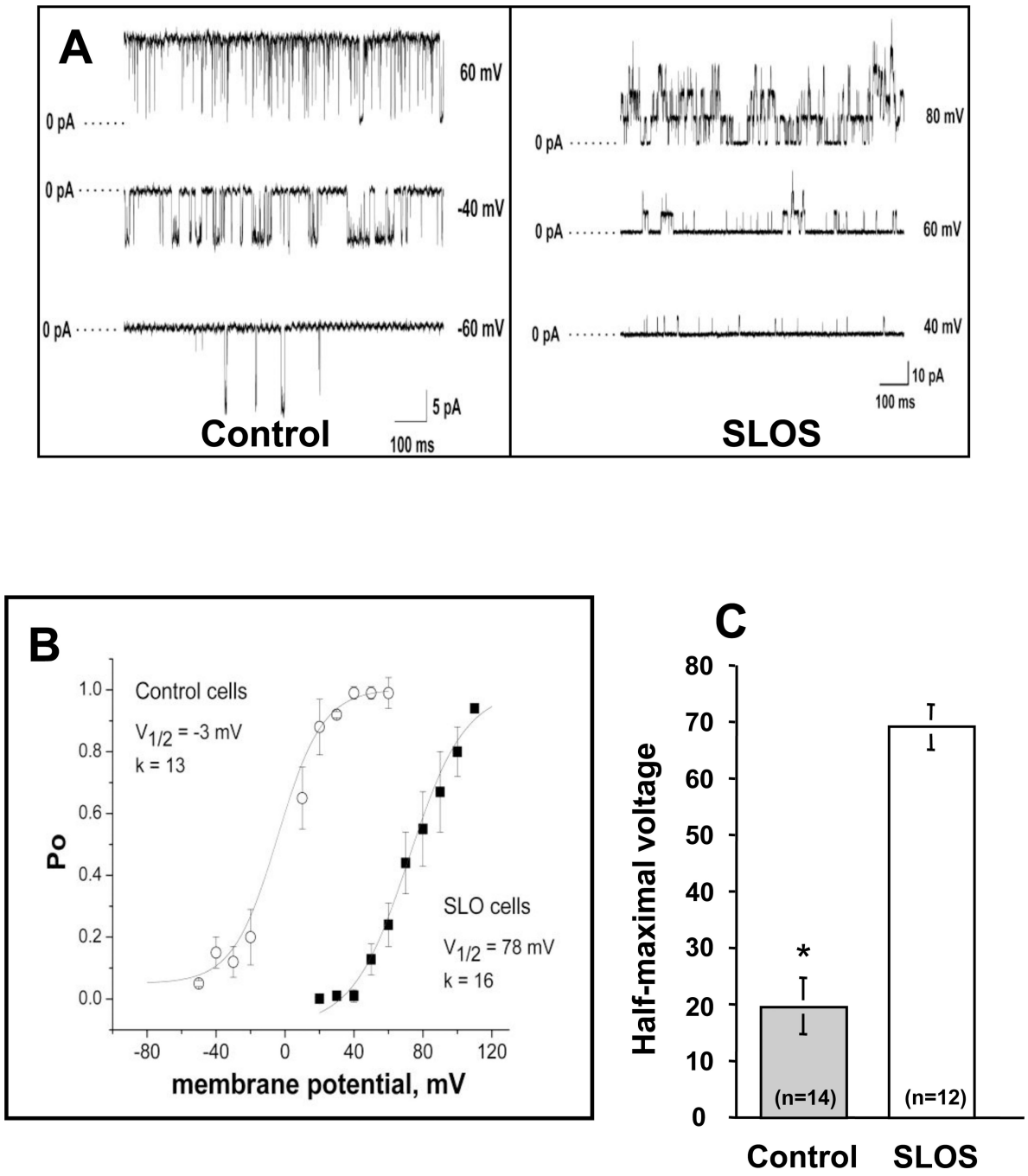

Figure 7. Altered BK_{Ca} channel activity in SLOS cells

(A) Single-channel, inside-out patch clamp recordings of BK_{Ca} currents in control and SLOS cells, measured at different voltages as indicated to the right of each trace. Data were sampled at 10 kHz and filtered at 5 kHz during acquisition. **(B)** Voltage-activation curves of the BK_{Ca} channels measured in control and SLOS fibroblasts. Channel open channel probability (P_o) is plotted as a function of membrane potential. The lines represent a least squares-fit of a Boltzmann function where $P_o = P_o max/[1 + exp((V_{1/2} - V_m)/k)]$, $P_o max$ is the maximum open probability, V_m is the membrane potential, $V_{1/2}$ is the midpoint potential for activation, and k is a slope factor. Data represent average values from six different cells

from one typical control and one typical SLOS subject (Mean ± SD of cells). **(C)** Average difference in $V_{1/2}$ between all control (n=5 patients) and all SLOS (n=6 patients) with 4–5 measurements in each subject cell line (total measurements indicated in each group).

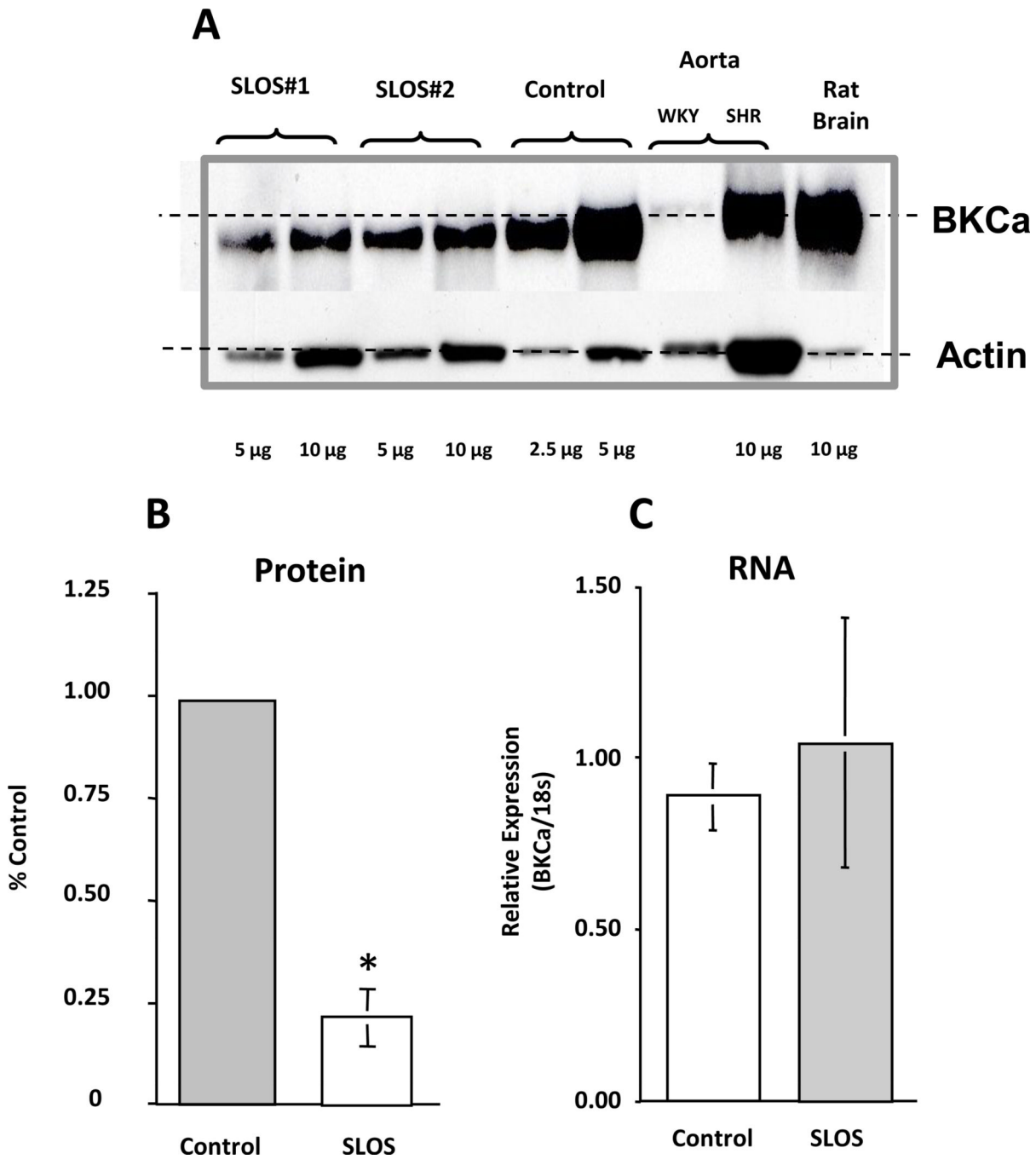

Figure 8. Reduced BK_{Ca} protein in SLOS cells

(A) Immunoblot of BK_{Ca} protein isolated from SLOS and control fibroblasts compared with rat aorta and brain (positive controls). Note the low level of expression of BK_{Ca} in the aorta from normal animals, but present in the aorta from hypertensive animals (SHR) at high levels, a finding described previously [50]. Protein loading was performed as indicated with β actin serving as a loading control. (B) Quantitation of BK_{Ca} protein from control (n=3 patients) and SLOS (n=6 patients) cells demonstrates a marked decrease in BK_{Ca} protein from SLOS cells. (C) Quantitation of BK_{Ca} mRNA by qPCR from control (n=3 patients) and SLOS (n=6 patients) cells shows no difference between control and SLOS BK_{Ca} mRNA levels. $*p < 0.01$

Table I

SLOS genotypes

SLOS cell genotypes used in study.

SLOS genotypes				
SLOS Patient	**Nucleotide change #1**	**Amino acid change #1**	**Nucleotide change#2**	**Amino acid change#2**
1	c.151C>T	p.P51S	c.964-1G>C	Splice site
2	c.740C>T	p.A247V	c.964-1G>C	Splice site
3	c.461C>T	p.T154M	c.964-1G>C	Splice site
4	c.906C>G	p.F302L	c.1409T>A	p.L470Q
5	c.278C>T	p.T93M	c.964-1G>C	Splice site
6	c.717C>A	p.F239L	c.976G>T	p.V236L